Experimental investigation of hot-wire laser deposition for the additive manufacturing of titanium parts

Materials Research Express

PAPER

Experimental investigation of hot-wire laser deposition for the additive manufacturing of titanium parts

Nirut Naksuk*, Pattarawadee Poolperm*, Jiradech Nakngoenthong*, Waravut Printrakoon* and Rattanapon Yuttawiriya*

Automation for Material Processing Research Team, Material Processing and Manufacturing Automation Research Group at the National Metal and Materials Technology Center (MTEC), National Science and Technology Development Agency (NSTDA), Thailand Science Park, Pathum Thani, Thailand

* Authors to whom any correspondence should be addressed.

E-mail: nirutn@mtec.or.th, pattarawadee.poo@ncr.nstda.or.th, jiradecn@mtec.or.th, waravutp@mtec.or.th and rattanapon.yut@mtec.or.th

Keywords: laser welding, wire feed, additive manufacturing, titanium alloy grade 2, hot-wire process, physical and mechanical properties

OPEN ACCESS

RECEIVED
21 March 2022

REVISED
4 May 2022

ACCEPTED FOR PUBLICATION
11 May 2022

PUBLISHED
24 May 2022

Abstract

Hot-wire laser welding is additive manufacturing (AM) technique that allows for the direct creation of complicated objects by melting layers of wire. This process is characterized by the use of hot-wire process, unification with the laser welding (LW) process in AM process. The empirical investigation of AM employing a hot-wire laser welding on a titanium alloy (grade 2) workpiece is presented in this research. There are three parameters in the hot-wire laser process namely wire current, welding speed, and wire feeding speed; this research examined porosities, microhardness, tensile stress, and residual stress. The filler metal used titanium AMS (American welding society) 4951F welding wire of grade 2 and measures 1.6 mm in diameter. Finally, the suitable hot wire laser welding parameters should be 0.183 cm s^{-1} for the welding speed, the wire current of 40 A, and the wire feeding speed of 1.00 m min^{-1} are 0.183 cm s^{-1} for welding speed, 40 A for wire current, and 1.00 m min^{-1} for wire feeding speed, which will give the average Vicker microhardness of 321.00–345.80 HV, the average tensile strength of 432.02 MPa (substrate); 670.30 MPa (horizontal direction), 497.39 MPa (vertical direction).

1. Introductions

The AM process refers to technologies that employ to fabricate the three-dimensional object layer by layer using powder, wire, or each other in the forming [1]. This wire AM process is capable of producing massive metallic components along with high production rates, low waste of material, reduced manufacture time, and created complicated parts with near-net shape [2] in comparison to traditional production technologies. For the deposition of wire metal, the deposited metal is created as a bead into the desired pattern (side by side or layer by layer) for the manufacture of perfect parts including the additional features of the parts. The direct metal deposition, [3–5] either powders or wires will are straightly melted into the power source created by laser beam, laser, electric arc, etc Currently, the wire AM process is applied for a variety of welding applications for titanium alloy fabrication in order to obtain better-quality parts than traditional manufacturing. From the point of view of the heat source, gas tungsten arc welding [6–8], plasma welding [9], and gas metal arc welding [10], their high deposition rate and the cheap cost are regarded as viable options for the manufacture of massive metal components as demonstrated by Ding (2016) [11]. Meanwhile, laser beam melting [12], laser welding [13], and electron beam melting [14], attempt to improve production efficiency and geometric complexity. For laser, the deposition majority are used to repair damaged or worn parts and formed workpieces printing ranging from small to large depends on metal the wire or the powder [15]. During AM process, the transient heats and metal flows (fluid) are pivotal because they affect the as-constructed microstructure [4]. Recent research has focused on features of as-built microstructures, mechanical characteristics, optimization of deposition conditions, and age hardening heat-treatments of deposited welding [16]. Nevertheless,

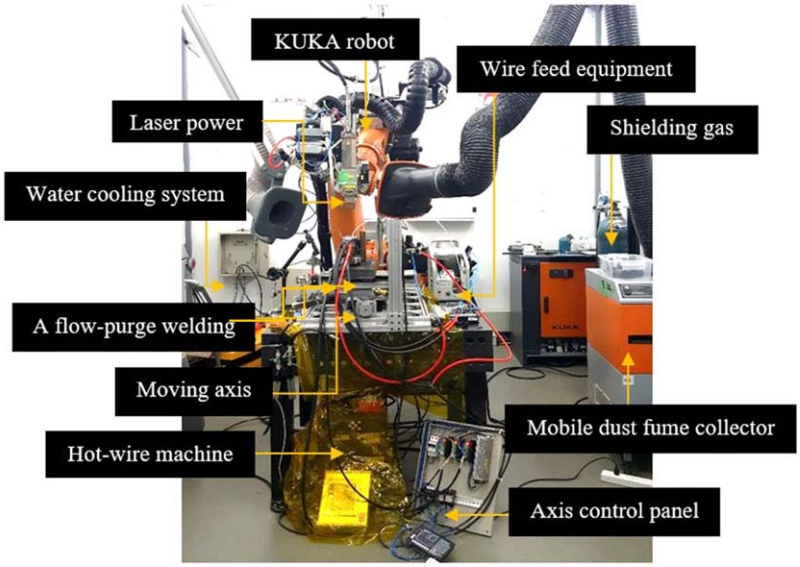

Figure 1. Experimental set up for AM process system.

Table 1. Chemical composition for titanium alloy grade 2.

Elements	Standard (% w w)$^{-1}$
C	0.08–0.10
Fe	0.30
H	0.015
N	0.03
O	0.25
Ti	Balance

the precision and surface quality are normally poorer than machined workpieces. To satisfy the needs of the aerospace [17], automotive [18], fast tooling industry [19], teel industry, and various metal parts which require high strength, the current focus of AM processes development have recently switched to fabricating the complicated shaped metal component, particularly titanium alloy material which is seldom manufactured in general industry and economically [20].

In titanium alloy, residual stresses have a considerable impact on the strength of welded structures including influence on welded component performance and often impair fatigue properties. The merger of welding residual stress with working stress [21] underlying engineering elements and structure can cause failure. Even though the combination of processes has shown great potential so far, the process's inherent problems such as warping because of thermal stress pose a serious obstacle to its wide application. As a result, it is vital to establish a continuous process for optimal heat management and higher speed. High-energy-density welding methods used to generate full single pass autogenous welds (titanium alloys materials) are preferable to welds that require multi-pass operations [22], which this comparison is based on the material chosen. The high cooling rates associated with welding processes with a high energy density like electron beam and laser beam welding can result in the fusion zone microstructure that exhibits poor strength and is prone to breakage. Chiefly, plasma welding is considered high-energy-density welding which is preferred for successful titanium welding as compared to other existing AM methods, i.e., electron beam welding and laser beam welding, etc [22]. In addition, Leyens [23] cites a lamellar microstructure, as a result of which easy cooling from temperatures higher than beta temperature. The microstructures are fine or coarse depending on the cooling rate, moreover, when the cooling rate is lowered, the lamellae microstructures grow coarser for titanium alloy material.

The hot-wire technique involves passing a current through filler wire and heating the filler wire to built-up metal parts. In other words, the filler wire melted liberally from the arc heat source that melted the base metal. Thus, the rate of deposition may be controlled [24]. The hot wire procedure will be used when a high deposition of filler wire is required [25]. The feeding of cold wire has some disadvantages. During conventional welding, the deposition rate is slow because the wire is cold wire, and no current through it. A portion of the laser power is

Table 2. Mechanical properties of the titanium alloy grade 2.

Mechanical properties	Standard value
Average tensile strength	485 MPa
Yield strength (0.2% offset)	275–448 MPa
Elongation (% EL)	18%–20%
Hardness Vickers	160–200 HV
Modulus of elasticity	103 GPa

Table 3. The settings for the hot-wire laser welding process.

Variables	Details	Unit
Laser type	Fiber laser	—
Fiber cable size	400	μm
Laser power	3	kW
Angle of laser irradiation	Vertical	—
Angle of wire feeding	45	Deg
Position of wire feeding	1	mm
Wire feeding speed	0.80–3.60	m min^{-1}
Wire current	40–70	A
Spot size/spot diameter	7.85	mm
Welding speed	1.83–5.00	mm s^{-1}
Shielding gas	25 (Ar)	l min^{-1}
Laser lens distance (front lens) to the workpiece	346	mm

absorbed by the melting of a cold wire. Normally, to atone for the energy lost in melting the cold-wire, welding speed is often sacrificed (reduced) [26]. According to reference Kota (2010) discovered that LHW has tremendous potential for high efficiencies, such as welding speed and high deposition rate, as well as excellent quality, such as low deformation [27]. While [13] observed that using a hot-wire increased the gap-bridging performance of laser welding and considerably reduced the laser power required for the penetration deep of the weld to be achieved. From the foregoing, the hot-wire process has been used to its advantage in many instances.

This study describes the hot-wire laser welding technique for measuring porosity, microhardness, tensile strength, and residual stress. Besides, the required settings for the hot-wire laser welding process are achieved, allowing the titanium alloy welding workpiece to have microhardness and tensile strength within accepted or good mechanical properties. The requirements for good mechanical properties of titanium alloy resulted in an excellent balance of medium strength and quite good ductileness.

2. The experiment setup: machine preparation and methods

2.1. Material and method

The titanium alloy grade 2 substrate in this investigation was cut to dimensions of 135 mm width, 350 mm length, and 10 mm thickness. As a filler metal, titanium AMS 4951F of grade 2 welding wire with a 1.6 mm diameter was employed. The chemical composition is measured from Shimadzu brand by EDX-8000: Energy dispersive x-ray fluorescence spectrometer as well as the mechanical property values [28–31], shown in tables 1 and 2.

The workpieces are firmly secured to the device of mechanical clamping all along the hot-wire laser welding process to prevent sliding or deviating Laser welding is also used hot-wire in the deposited process. The hot-wire welding was carried out with the help of a KUKA robot's robotic welding system. The welding movement relative to the substrate was generated using a six-degree-of-freedom KUKA industrial robot arm, which is a very flexible and versatile robot. Figure 1 presents the setup, which includes a welding axis, substrate plate, hot-wire process, shielding gas, KUKA robot, camera, jigs, etc table 3 shows the variables of hot-wire laser welding employed in this study.

2.2. Methodology

The first part starts with qualitative research, which included an interview to determine the composition and performance metrics. The data were gathered through conversations, questions, and face-to-face interactions between interviewers with staff and researchers, which have knowledge and expertise in welding and various

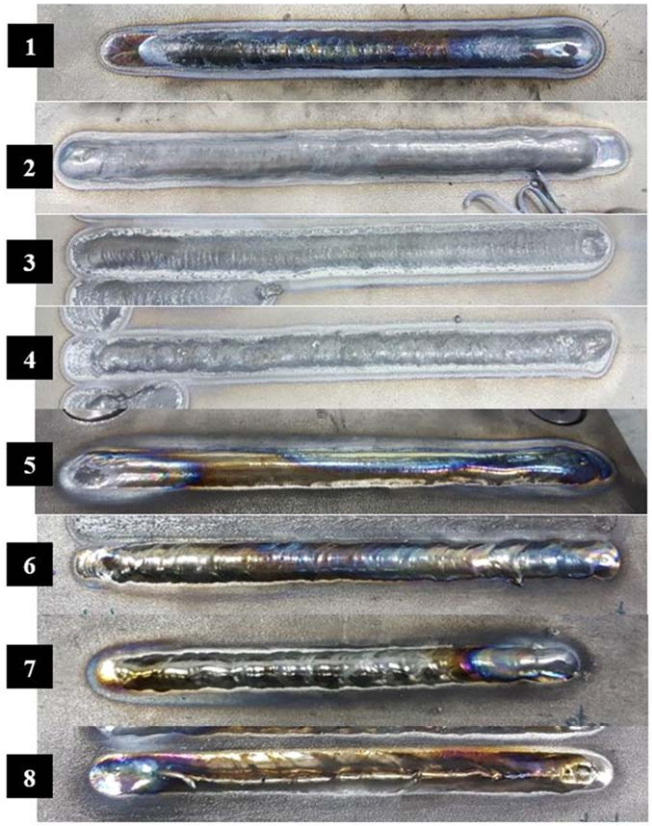

Figure 2. The deposition of single beads for a designed experiment for a hot-wire laser welding procedure (Numbers 1–8).

Table 4. The welding experimental conditions of eight welding specimens.

			Hot-wire			
No.	Welding length [mm]	Welding speed [cm s]$^{-1}$	Wire feed speed [m min]$^{-1}$	Wire current Amperage: [A]	Reverse feed speed [m min]$^{-1}$	Reverse feed speed [s.]
1	140	0.400	3.60	50	5.00	0.50
2		0.400	3.60	70		
3		0.183	0.80	40		
4		0.500	3.60	70		
5		0.183	1.00	40		
6		0.250	0.80	40		
7		0.200	1.00	40		
8		0.250	1.00	40		

metals, reaching the possibility of suitable parameters for the test. In another research, Kota (2010) used the welding conditions i.e., 0.3 m min^{-1} of welding speed, 3 kW of laser power, 70–149 A of wire current, and 0.8–3.6 m min^{-1} of wire feeding speed [32]. While Zhu (2021) applied 3.3–5.5 kW of laser power, 6–20 m min^{-1} of wire feeding speed, and 0.24–0.5 m min^{-1} of welding speed for hot-wire laser method [33]. As a parameter, the laser power, wire feeding rate, and welding speed were all varied respectively. Other control parameters that may affect the forming of the workpiece must consider together. So, we have to do a preliminary experiment to find parameters that affect the forming of the metal AM process. The parameters selected in this study are welding speed, wire current, and wire feeding speed. The second part is quantitative research. By synthesizing the information obtained from the interview as a component. The experiment design was used to create 2^3 full factorial designs (8 trials with 3 variables and 2 levels) of hot-wire laser welding processes by statistical analysis software (MINITAB). Table 4 shows the welding experimental conditions of eight welding specimens for the hot-wire laser welding process. Figure 2 depicts an instance of a picture derived from the results of the designed experiment (all 8 trials).

Figure 3. The trailing shield device.

From the visual inspection of the welding quality, the quality of the welds determines the capacity to support applications such as strength, corrosion resistance, size, and shape. These characteristics are based on the welding materials and the conditions that occur during welding. While cracks, undercuts, overlaps, porosities and slag inclusions, and incomplete fusions are all examples of defects that may be visually assessed on a weld [34]. Although this is a simple test method, it requires knowledge and skills. there is no standard to determine whether it is a defect and can only be tested on the surface.

Other than the above criteria, the degree of atmospheric contamination will be indicated by the surface discoloration. The oxide layer causes the color change on these titanium alloys, which degrades the mechanical qualities of the workpieces or makes them worthless, as well as increases the cost [35]. The creation of the oxide layer causes the metal's surface to change color. The built-up deposited welding will be vivid and silvery under ideal shielding conditions. As the contamination level rises, the color varies from light straw, dark straw, dark blue, and light blue eventually to powdery white, etc The mild contaminations are indicated by the color of light straw and dark straw, which are generally acceptable. The dark blue color signifies a higher level of contamination, which may be acceptable depending on the terms of use or service. Meanwhile, the light blue, grey, and white colors show a significant amount of contamination that they are considered undesirable [36]. Contamination from previous layer welds will affect all subsequent welds in the multiple pass welding. Another basic test, such as the bending test, is a dependable but damaging form of inspection. The single welding bead has bright, silvery, and light straw colors for single bead number 5, which is normally acceptable. In addition to the color changed criteria, the single bead number 5 had a superior appearance and form when compared to the other welds and the filler wire was not an issue, with no interruptions, splashes, or jerky movement above all. While the wire was being drawn back, the wire tip did not cling to the ceramic or copper tip (wire support made of ceramic or copper rod). To obtain good mechanical and physical properties in a workpiece (titanium material), including an outstanding balance of moderate strength and relatively good ductility, thus these single beads for the welding process were implemented. An infrared camera (IR) was used to measure the temperature on the surface of each layer at the mid-point of each welded bead layer. After a thirty-minute break, the deposition process resumed deposited welding.

As can be seen from figure 2, the degree of oxidation is different from the start to the end of the welded beads because we designed a trailing shield device for use in the hot-wire laser welding process. It is known that titanium material, a protected environment is necessary during the welding process. The argon gas was used in this study because of its low ionization potential, ease, and reliability [23] resulting in arc stability. While

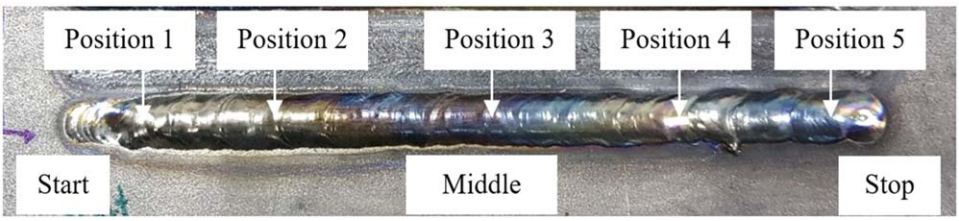

Figure 4. Positions for measuring bead height and bead width of deposited weld.

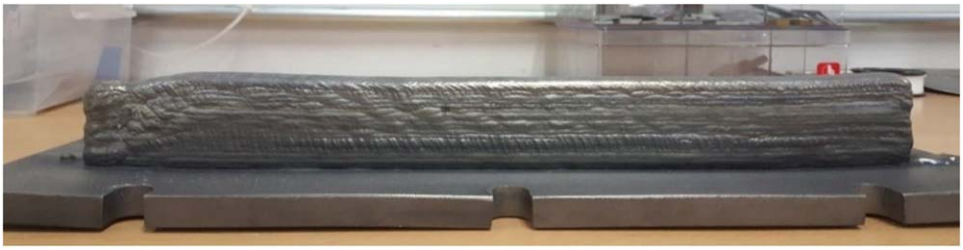

Figure 5. Photographs of the deposited walls: 20 layers.

applying the trailing device can help to boost the process's flexibility and more convenient for movement. It's a shielding device that keeps the argon shielding of the hot-welded metal till it cools to a safe temperature, which atmospheric contamination is not a concern. However, compared to welding with a closed system (in a gas chamber), which is made of a non-gas-permeable material for delicate applications, the use of the trailing shield device still contaminates the atmosphere and causes oxidation due to the susceptibility of titanium to oxygen, nitrogen, and hydrogen. So, the workpiece was found to have a degree of high oxidation at the start and the end of the welded bead by reason of the shielding gas (argon gas) is not enough for all protecting the weld and workpiece to flush the air out including the use of trailing shield devices that are not sufficiently comprehensive. Figure 3 is an example of a shielding device utilized in the hot-wire laser welding process.

This study did not use a strategy of zig-zag deposition, using linear deposited motion or linear path of the robot movement. The built-up welding at the start and the end of each layer are at the same points. Figure 4 shows the placement of the bead (height and width) measurements for hot-wire plasma welding process. The height of each layer was measured in 5 locations using a vernier caliper and welding gauge to measure the height from the baseplate up. Bring these values to find the average per layer which will be used as the height value of the robot that will need to be lifted to the next layer.

The deposited wall was subjected to the welding condition of single bead number 5. The process was operated at 0.183 cm s^{-1} of a welding speed, 1.00 m min^{-1} of a wire feeding speed, 40 A of a wire current, 5 m min^{-1} (0.50 s) of a reverse wire feed speed, as well as illustrated in figure 5, the final dimensions of the wall are the length of 300 mm and the height of 36.00 mm after 20 layers of deposition. The graph in figure 6 depicts the values of bead height of titanium alloy walls constructed using the hot-wire laser welding procedure. The figure can be described in detail as follows: the blue line, the pink line, the gray line, the yellow line, and the purple line, which displays the weld bead height in positions 1–5, respectively. At the same time, the green and red lines represented the arc distance height and the average bead height.

In the literature review, in reference Mok (2008), it was discovered that titanium alloy deposition utilizing a high-power diode laser and wire at a chosen wire feed rate of 1.2 and 2.06 kW for laser power, welding speed generally varies from 0.05 to 2.4 m min^{-1} for the deposition of titanium alloy [37]. Mortello (2021) examined titanium wall construction in wire laser-AM, in which the process parameters namely 300 W of laser power, the diameter of beam spot 1 mm, 8 mm s^{-1} of travel speed, and 15 mm s^{-1} of wire feed speed at 15-layers deposition [38]. According to [33] investigate the suitable circumstances of AM utilizing a hot-wire laser that is a merger of a high-power diode laser with a system of hot-wires. The process conditions were 3.3–5.5 kW of laser power, 6–20 m min^{-1} of wire feed speed, 20–40 of wire feed rate, 45 degrees of wire feeding angle, and 30 l min^{-1} of shielding gas (Argon). The Z3321-YS308L with a 1.2 mm diameter was used as a filler material but the practical height was more than 50 mm, 55 mm of the maximum height, and 8 mm of the practical width with extremely high efficiency utilizing 15 layers.

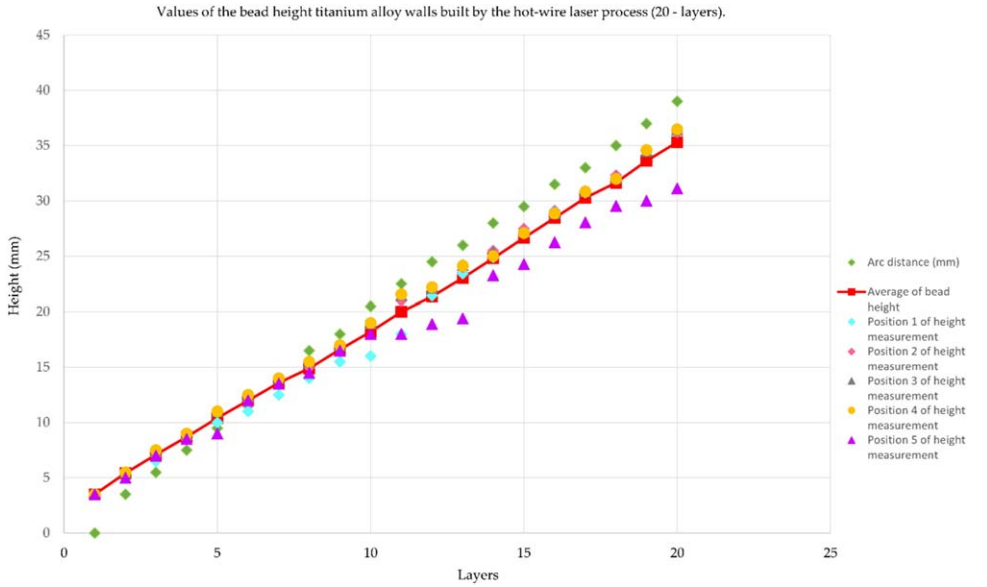

Figure 6. The bead height values of titanium wall (20-layers) constructed by hot-wire laser welding method.

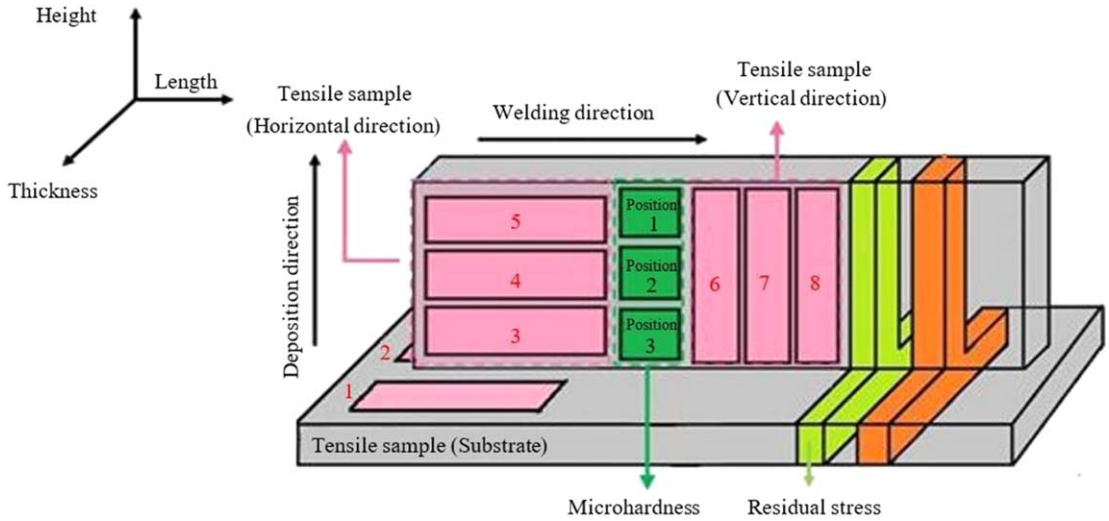

Figure 7. Separation of welded workpieces.

Once the hot-wire laser welding procedure has been finished in accordance with the design of experiments. Figure 7 comprises four sections of the AM workpieces in the experiment (porosities, Vickers' microhardness, tensile strength, and residual stress). The workpiece before segmentation to measure various properties (whole piece) will be tested for porosity and define the size or position of the pores that occur in the welds. Porosity testing uses the machine brand, the GE Phoenix V|tome|X S employs a high-power nano focus x-ray tube in conjunction with a 240 kV/320 W microfocus x-ray tube. The pore, also known as a cave pocket, is a typical welding feature that occurs often during the welding process. The cracks can also occur during the welding process for AM. The crack type is mostly dependent on its solidification and is typically motivated by the hindrance of solidified grain movement or excessive strain at the melting pool [39, 40].

The second part of welded workpiece brings grinding, polishing, and mounting of the cut workpiece in resin. The abrasive with sandpaper grades 120, 400, 600, 800, 1000, 1200, 2500, and 4000, respectively. The Vicker microhardness uses the machine brand, HMV-G Microhardness Vickers Hardness Tester, Model: HMV-G31FAD-HC, S/N I631258G0105. The square examples were obtained in the direction of transverse near the center of layer bands like the top, middle, and bottom areas of the deposited wall [41]. Each position was measured five-time these measurements were calculated and graphically displayed. The parameters applied are force is about 1.961 Newtons or HV0.2, loading speed 1 g s^{-1}, and held for 10 seconds. Tensile strength will be

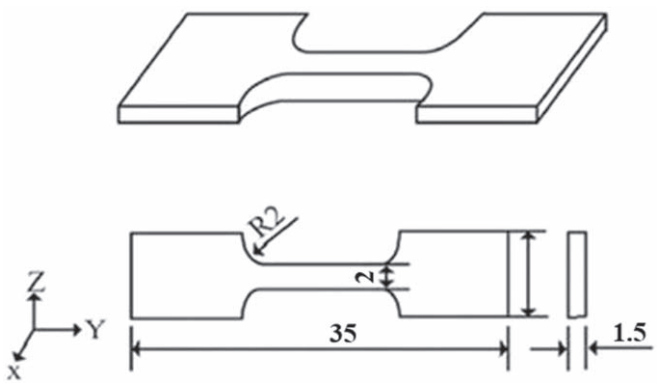

Figure 8. Tensile specimen dimensions (in millimeters).

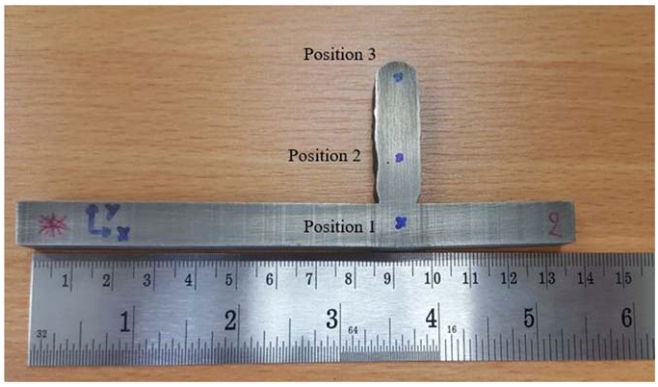

Figure 9. The specimen and location utilized to determine residual stress.

measured on the third section of the welded workpiece using ASTM-E8 for metal. Tensile strength testing for specimens was performed by the machine brand, universal testing machine of Instron 8872, S/N 3367/09. Each wall's sample positions were divided into sections. The three tensile test specimens were obtained equidistantly in accordance with the vertical direction from the middle until the end of the deposited wall. Meanwhile, the three tensile test specimens were taken uniformly from the top until the bottom [14], as well as the other two tensile test specimens in the substrate. Figure 8 depicts the tensile specimen dimensions in millimeters.

The residual stress will be assessed on the fourth part for each welded workpiece. Residual stresses in titanium alloy, which normally deteriorate fatigue properties, can have a significant impact on the performance of welded components. As a result, it's crucial to manage stress under control and monitor it. The residual stress was determined by measuring the longitudinal and transverse stresses on the surface using the non-destructive x-ray diffraction (XRD) technique for metals. The x-ray residual stress analyzer of μ-X360s portable from Pulstec was used to assess the residual stress of the welding specimen. The machine employs XRD analysis and the cos alpha method technique. This analyzer is a low-cost, high-speed, and high-precision measuring device with numerical control in 2 directions for the precise movement of x-ray sensors, etc Residual stresses can be computed from comparing the entire x-ray debye ring with the non-stressed condition, The cos α technique, also known as the single-exposure approach relies on a two-dimensional detector to calculate stresses and capture the ensuing diffraction cone of a single incident x-ray beam [42–44]. The Debye–Scherrer ring is formed by the intersection of the diffraction cone and the area detector. Figure 9 depicts the specimen and location utilized to quantify the residual stress of a hot-wire laser welding process. Table 5 shows the requirements for measuring residual stress.

3. Results and discussion

3.1. Porosity

Figures 10(a)–(c) represents porosity in an AM component sample: (a) front area, (b) middle area, and (c) back area. The multilayer deposition had a dense structure and was slightly porous at the commencement of the

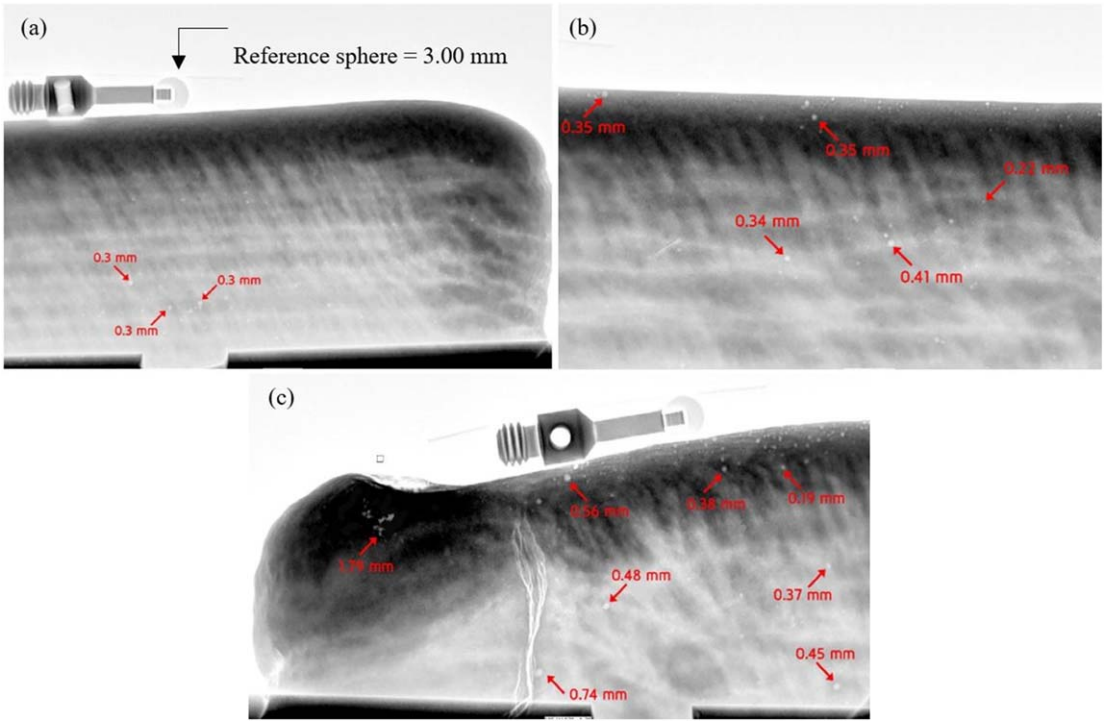

Figure 10. Porosity volume: (a) front area; (b) middle area; and (c) back area.

Table 5. Specifications for residual stress measurement.

Lists	Details
Item	μ-x360s
Collimator size/Spot size	Standard: ø 1.0 mm (Illuminated surface: approx. ø 2.0 mm)
Maximum measurement distance	Max 150 mm
x-ray tube voltage & current	30 KV/ 1.5 mA max.
x-ray tube	Cr/ Co/ Cu/ V/ Mn
Method of measurement	Cos α
Measurement item	Residual stress/FWHM/Retained austenite (optional)
Target material	Ferrite, aluminium, nickel, titanium, ceramics, etc
Weight	Sensor unit: approx. 2.4 kg Power supply unit: approx. 6.2 kg
Measurement time	60 secs/measurement point

welding operation. A maximum porosity size of 0.30 mm was found in the front region. While in the middle area, the highest and lowest porous diameters were 0.41 mm, and 0.22 mm, respectively. Furthermore, the greatest porous size in the back area was 1.79 mm, and the smallest porous size was 0.19 mm. Higher pore densities for most AM parts are distributed in the upper area of the workpieces along the deposited weldment at the middle and the end of the welding process, resulting in a high accumulative temperature. Moreover, the depositions appear to fracture at the end of the welded, as shown in figure 10(c). The power source and welding speed are constantly resulting in the cooling rate being poor, oxygen accumulating, and cracks occurring in the surface of the back area for the workpiece. At the same time, the trailing shield device was used in AM process (welding each layer) for hot-wire laser welding, in which there may be oxygen in the welding workpiece and there are fewer cooling areas when a higher welding layer. For fracture surfaces analysis, we have not analyzed the fracture surface since we focus on the appropriate parameters and full forming process, afterward to improve the mechanical and physical properties later. In this study, the measurement of various properties of the specimen will remove the cracked part, which is not used for analysis.

The pores are a common feature of welding and may be found in practically all forms of welding. High porosity is a common problem in metal AM techniques which greatly depends on the processes, however, these porosities may occur throughout the printing process when holes, cavities, or other factors are produced inside the workpieces. If there are a lot of pores, the workpiece's density will be decreased. They can also have a direct impact on a part's mechanical qualities, rendering it more susceptible to fractures and other damage, especially

Table 6. Results of Vickers microhardness for the hot-wire laser welding process.

Samples	Locations (MPa) 1	Average 2	3	4	5		SD.
Position 1	317.00	335.00	314.00	314.00	325.00	321.00	9.00
Position 2	350.00	318.00	353.00	352.00	319.00	338.40	18.20
Position 3	362.00	343.00	329.00	344.00	351.00	345.80	12.10

when subjected to high loads. According to reference [45] found that the porosity and cracks can be seen in several areas of the workpiece by using x-ray computed tomography. As the thickness of β-phase areas decreases, they are unable to absorb enough energy and fracture propagation retard. While [46] offered an ultrasonic technique of measurements for metal AM process control, which the RT image showed the pores near the center at a max of 15.62% porosity. In wire arc AM of aluminum or another material can be found many small pores (less than 50 mm in diameter) [47]. The small pores float up during solidification due to reduce pressure and can merge into bigger ones, that may be found towards the top of each deposited layer. Nevertheless, the excessive plasma and laser energy, on the other hand, might cause melted material droplets to spatter, resulting in pores [48]. The solubility of a gas in a liquid metal decrease as the cooling rate of the gas flows out of the solution in the character of bubbles [22]. Furthermore, because the dendritic solidification interface and pores function as stress risers that generate brittle fractures and enhance the susceptibility to failure, the porosity will grow increased [49]. The escape of pores investigated by [50] was caused by the flat-position welding, the slow welding speeds, and uphill in the vertical position. Meanwhile, our results are based on the x-ray computed tomography method for this measurement. On the other hand, the volumes of porosity are sometimes desirable such as in certain biomedical implants since the pores promote better osseointegration with biological tissue [45, 46]. These requirements need porosity monitoring capability where the level of porosity in a part can be measured after being built.

The root of porosity is the portion of root volume absorbed by the surrounding air, nitrogen, oxygen, hydrogen, and contamination in the melting pool. Many factors influence these. In this study, includes the bulk density of the surrounding surface, root growth rate, availability of inert gas (argon gas) to shield the specimen and root, temperature, etc The increased root of porosity is ordinarily the result of the presence of oxygen and contaminants into the roots. At the same time, there is not enough shielding gas in the rear weld because of the applied trailing shield device, thus, oxygen can interfere and cause porosity.

3.2. Microhardness

Table 6 displays the Vickers microhardness values for the hot-wire laser welding technique. From the substrate to the top area, Vickers microhardness coupons were incised from the produced thin wall, with a stable value of around 314.00–335.00 HV from 15 mm (position 3), 318.00–353.00 HV from 25 mm (position 2), and 329.00–362.00 HV from 31 mm (position 1). Furthermore, the overall average was 321.00–345.80 HV. Specimens 1, 2, and 3 were finished with a waiting period of 30–40 min and a force of 200 g. The hardness test was carried out in accordance with ASTM specifications standard test method E92. The typical Vickers microhardness values of the deposited layers were reported to be about 160–200 HV for titanium alloy grade 2 [51, 52]. We found that the average deposit Vickers microhardness values have a higher value than the standard value of titanium alloy, moreover, sample position 3 was greater than that of sample position 2 and sample position 1.

The hardness distributions for different intermediate times between the layers in the deposit-build condition by the example. Hardness values ranged from 321.00 to 345.80 HV showing significant dependency on the deposited (built-up) height of hardness values on temperature distribution. Vickers microhardness is utilized for hardness analysis since it is a procedure that can be applied to all materials. Vickers Hardness may be measured from 10 HV to 2000 HV [53]. Vickers microhardness values of 345 to 350 HV were reported by [54]. Meanwhile, the results reported Sun Rujian (2018) used the Vickers microhardness tester with a test weight of 200 g and a dwell period of 10 s to investigate the evolution of micro-hardness between 75 and 110 HV [55]. Besides, Vickers microhardness tests were done in the base material, at the wall substrate, and along the wall's constructing direction [38], according to Mortello M (2021). In terms of measurement, the difference in hardness between the top and bottom regions isn't equal. According to the reference by [41], the volume of wear is inversely proportional to the material's hardness, thus the lower hardness materials during wear caused more plastic deformation on the surface and beneath the surface, resulting in deeper fractures and delamination [56]. The top layer (position 1) has a lower hardness than the other layers. The increase in dendritic structures observed with increasing deposit height is the direct source of the reduced hardness. The hardness gradients are expected at

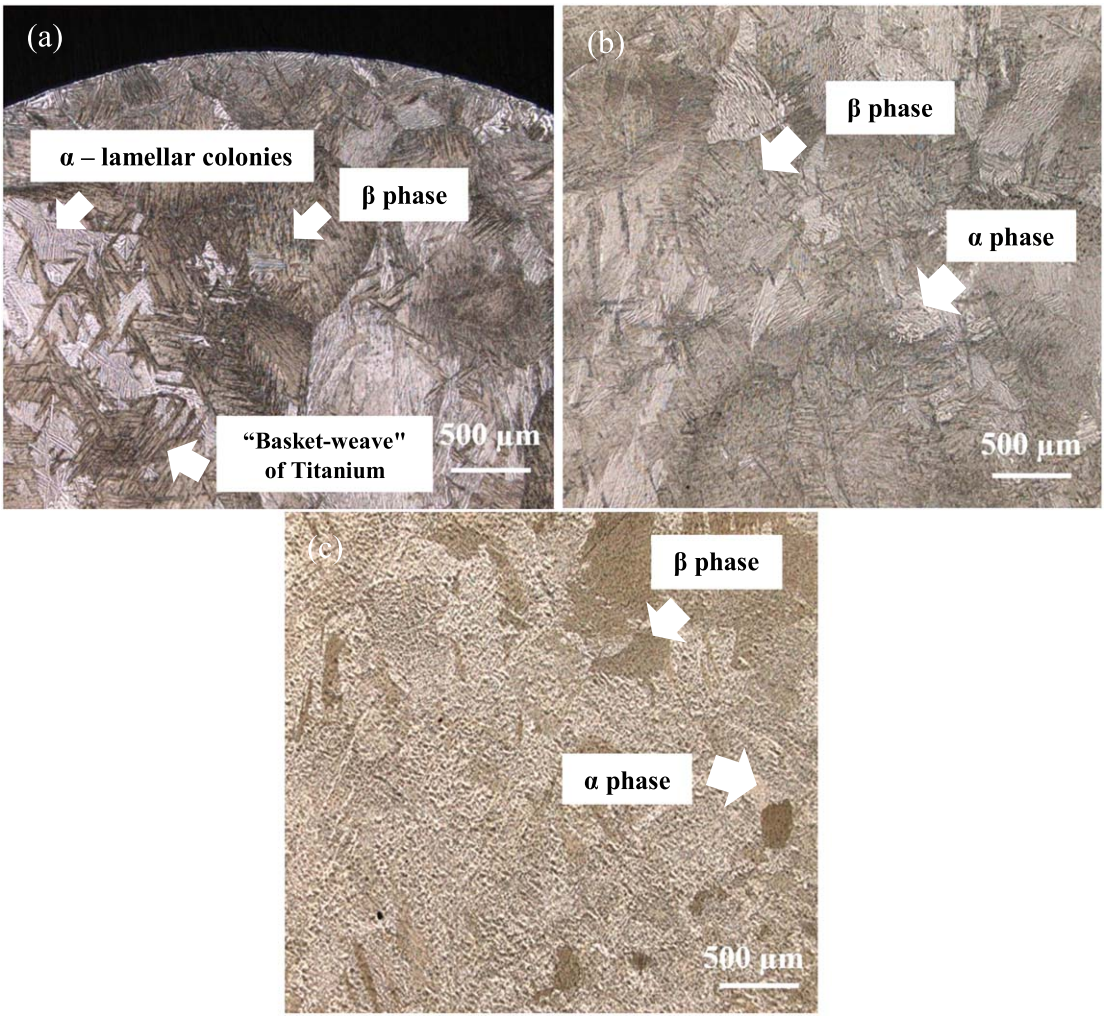

Figure 11. Microstructure of (a) top, (b) middle, and (c) bottom areas of deposited wall.

deposits as a result of each layer is a history of different thermal. The total heat created is uniformly and widely distributed throughout the material. From the result, we discovered that the hardness of the specimen reduces from bottom to top.

On the multilayer-welded specimens, Vickers microhardness tests were conducted to display possible missing heat treatment effects. All measurement positions have a similar form and value, with a higher hardness value near the substrate at the bottom and center areas, and a lower hardness value towards the top of the workpiece. In the hardness measurement of the metal workpiece, each measured positions have unequal hardness values because, in the structure of a material, there is not only one structure. For titanium materials that undergo the thermal welding process, the structure changes. Some positions are pressed to the matrix structure, the hardness is not very high. But when pressed to the phase in the structure, it was found that the hardness value immediately came up. Therefore, the resulting phase has more or less different values and sizes, which all affect the hardness. Figure 11 depicts the deposited microstructure in a cross-section vertical to the laser scanning direction for the hot-wire laser welding method. As the distance between the substrate and the welded deposit grain grows, the microstructure changes to a highly coarse microstructure with a big grain size. The welded deposition in positions a-c was distinguished by alpha (lighter portion) and beta grains (darker parts). Position (a) contains β phase, α—lamellar colonies, and is found the 'Basket-weave' or Widmanstätten microstructure of titanium alloy. The microstructure is refined when the cooling rate is raised, and α colony size and α-lamellae thickness are both reduced. The new colonies are also inclined to form on borders of other colonies, not simply on β-phase boundaries. Additionally, dendritic development and pore nucleation rate have a competitive relationship. The 'basket weave' or Widmanstätten microstructure of titanium is created as a result of the close relationship between porosity and grain size [47].

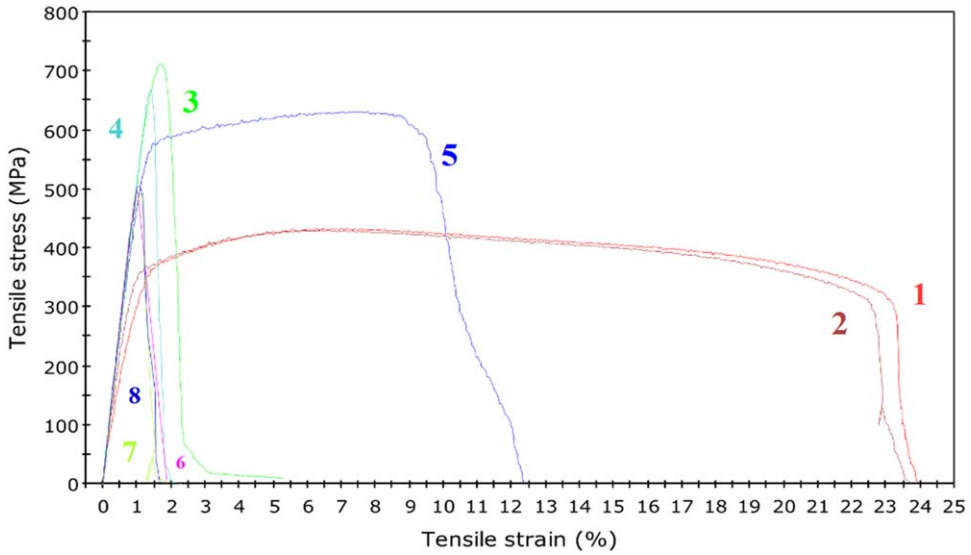

Figure 12. Engineering stress-strain graphs of specimens after deposited weld.

Table 7. As-deposited wall tensile strength results for the hot-wire laser welding.

No	Samples	Maximum load (N)	Modulus (Automatic young's) (GPa)	Tensile stress at yield (Offset 0.2%) (MPa)	Tensile strength (MPa)	Elongation at break (%)	Thickness (mm)	Width (mm)
1	Position 1	1459.41	43.50	250.64	433.57	11.91	1.65	2.04
2	Position 2	1441.84	50.75	318.71	430.46	10.88	1.65	2.03
3	Position 3	2305.56	53.08	681.24	711.59	12.32	1.62	2.00
4	Position 4	2184.85	51.83	649.96	667.66	11.99	1.62	2.02
5	Position 5	2056.75	54.80	519.66	631.64	12.07	1.62	2.01
6	Position 6	1636.60	53.50	466.86	494.60	11.03	1.63	2.03
7	Position 7	1630.21	49.41	481.92	492.68	11.30	1.63	2.03
8	Position 8	1652.19	56.45	503.84	504.89	11.23	1.62	2.02
Averages			Substrate (No. 1–2)		432.02	11.39		
			Horizontal direction (No. 3–5)		670.30	12.13		
			Vertical direction (No. 6–8)		497.39	11.19		

3.3. Tensile strength

For the hot-wire laser welding technique, each wall was sectioned (eight samples). The two tensile test samples are in the baseplate (numbers 1–2). Three samples of horizontal tensile testing by numbers 3–5. The other three tensile test samples (numbers 6–8) were taken in an even pattern in the vertical direction from the top to the bottom of each wall [49]. Table 7 and figure 12 show the results of tensile strength tests as well as eight-row plots of tensile strength. Depending on the heat treatment applied after the build-up and the test direction, which the average tensile strength value reaches 670.30 MPa (elongation 12.13%) for the horizontal direction, 497.39 MPa (elongation 11.19%) for the vertical direction, and 432.02 MPa (elongation 11.30%). Following welding, the engineering stress and engineering strain for specimens is demonstrated to have a similar relationship.

Moreover, the minimum and tensile strength values on average of titanium alloy grade 2 are 345 MPa and 485 MPa by the standard specification for titanium alloy (grade 2) [30]. The tensile strength values of the substrate are shown in graphs numbers 1 and 2 to be 430.46–433.57 MPa. Graphs numbers 3–5 show the values of tensile strength of the longitudinal area reach 631.64–711.59 MPa. Meanwhile, graphs numbers 6–8 show the values of tensile strength of the transverse area reach 492.68–504.89 MPa. It should be noted, however, that graphs 3, 4, and 5 (near substrate) have the highest tensile strength value when compared to the other graphs because the initial layers inherit the substrate's original fine-grained structure, as a result, their strength is greater than that of the remainder of the specimens. According to the result above, the tensile strength values of the vertical direction were lower than those of the horizontal direction (or the other directions) [30, 57], due to the neighboring deposited tracks' heat influence zone (HAZ) acting on each section in comparison to testing along

Table 8. Residual stress values.

Residual stress (MPa)			
	Measurement point		
	Position 1	Position 2	Position 3
X-axis (Longitudinal direction)	−312	849	540
Y-axis (Transverse direction)	−494	−968	508

the construction direction, tensile testing vertically to the build direction results in much lower ductility [58, 59]. In other research, they discovered that the produced distribution of residual stress and grain size in the depth direction were variables that may impact the tensile properties of the sheet thickness, as referenced in [60, 61]. The main causes of low tensile strength in workpieces were porosity and fracture. Furthermore, the effective sectional area of tensile specimens was decreased by porosity, fracture, and lowering the tensile strength [50]. The current study found that the main causes for the improvement in tensile properties are grain refinement and compressive residual stress layers on both sides of the workpieces [55]. As a result, the tensile strength and elongation of the longitudinal direction were greater than the transverse values.

The low modulus value, we found that this was caused by the deposited metal AM process (titanium material) of the hot wire laser welding, in which we may cut out the soft parts (weak) and too much under the surface for testing. As a result, the strength of the metal and the modulus are not higher than they should be. Besides that, the characteristics of the specimen being too small may not be suitable for direct modulus determination (maybe broken).

3.4. Residual stress

When the specimen is subjected to such extreme heat changes, it may cause residual stresses. Table 8 displays the residual stress along with the position of the reference samples. Residual stress values presented those measurements were both compressive stress (−) and tensile stress (+). The residual stress at position 2 was tensile (positive) in the longitudinal direction. The contact area between the bottom of a printed object has the biggest concentration of residual stress (in Position 2). The peak value of around 849 MPa is quite near to the deposited material's yield strength, which is between 810 and 870 MPa [62]. According to Ding [17], the deposition process causes uniform tensile stress in deposited walls. Even if tensile stresses persist throughout the welded deposition but residual stresses along the baseplate are lower because the regions are slightly compressive.

The fast solidification and subsequent thermal cycles cause part deformation. This has a detrimental influence on the component's mechanical properties, leading to a buildup of residual stresses in AM process. The cos α approach [3, 25] for measuring x-ray residual stress is the focus of this study. For many metals, the accuracy of the cos α technique for stress measurement has been verified to be comparable to the $\sin^2 \psi$ approach. Another, hole drilling method applying strain gauges to a sample's surface, drilling the blind or through holes to relieve stresses, calculating the initial residual stresses, and the stresses at the surface alleviated are all destructive techniques [63]. Recently, Hoye [64] have been measured large residual stresses in titanium of wire + arc additive manufacture components. Many physical phenomena are shared by AM and fusion welding, particularly the main physical factor that influences residual stress and distortion formation [65, 66]. In addition, we found that high-pressure rolling can potentially cause the requisite plastic strain for the release of residual stress in deposited weld [67]. The residual stress distribution was shifted significantly, and there were large compressive stresses as a result of this procedure. Moreover, the performance of welded components in titanium material can be substantially influenced by residual stresses, which generally deteriorate fatigue properties [22].

The residual stresses are higher than the ultimate tensile strength (UTS) of the tensile tests because the base plate used may be too thin which has a thickness of 10 mm, as well as, the base plate was securely clamped by jigs and fixtures to prevent it from moving while welding. At the same time, the hot wire laser welding uses high heat and does not allow the specimen to cool down freely, so, the base plate is bent/deflected and creates a lot of residual stress. Additional solutions may increase the thickness of the base plate. Moreover, peening is the process of working on metal surfaces to improve material property that aids in the reduction of stress concentration in the weld joints (press the welding line to loosen the workpiece before the next layer of welding). These methods will help to reduce stress stresses on molded parts.

4. Conclusions

On the basis of the analytical and experimental findings, the following conclusions can be reached.

(1) The suitable hot-wire laser welding conditions are 0.183 cm s^{-1} (1.83 mm s^{-1}) welding speed and 3 kW laser power on a surface. The suitable hot-wire temperature in the weld pool range was obtained using 40 A of hot-wire current, 1.00 m min^{-1} of wire feeding speed, and 5 m min^{-1} (0.50 s) of reverse feeding speed. After hot-wire laser welding, the wall widths were roughly (max) 6.00–12.46 mm in a single run.

(2) The voids in the workpiece (pores) are found in the deposits of the hot-wire laser welding process. Porosity indicates that the shielding device (including argon gas) was less than adequate and that unwanted gas-metal reactions are occurring. The pores, once formed, could persist through multiple layers or the whole pieces. The pores act as stress risers causing an increase in the susceptibility to brittle fracture. We discovered that the wall height grew, and the deposited rate of heat removal via conduction towards the baseplate dropped. While the temperatures will be better after the fixed interlayer and have a longer waiting time. Besides, when the wall height increases, so do the grain size (both increases and grows).

(3) As-deposited samples had a Vickers microhardness of 321.00–345.80 HV during the hot-wire laser welding process. The bottom area near the substrate had greater hardness than the other areas, because of the constituent of the phases and coarser microstructure at the top area of the workpiece

(4) Average tensile strength value reaches 670.30 MPa (elongation 12.13%) for the horizontal direction, 497.39 MPa (elongation 11.19%) for the vertical direction, and 432.02 MPa (elongation 11.30%).

(5) The annealing, strain hardening, and melting processes all affect the precision of calculating residual stress in titanium alloys. The cos alpha method technique and x-ray diffraction analysis were utilized to successfully determine the welding residual stresses in metal wall deposits. Tensile (positive) residual stress was found at positions 2 (849 MPa) and 3 (540 MPa), while compressive residual stress was at position 1 (−312 MPa) in the longitudinal direction.

(6) AM processes concern the high temperatures, which cause residual stresses to build up and subsequent distortions. So, heat management is one challenge associated with AM process. With the laser power at 3 kW throughout all welding lines and every layer, it causes the heat accumulation in each layer to rise. The consequences cause the laser workpiece to crack at the end of the workpiece. Because residual stress can frequently cause component deformation, cooling must be considered in the process.

Acknowledgments

The authors would like to thank the National Metal and Materials Technology Center (MTEC), National Science and Technology Development Agency (NSTDA), Thailand for financial, machinery, and equipment support.

Data availability statement

All data that support the findings of this study are included within the article (and any supplementary files).

ORCID iDs

Pattarawadee Poolperm https://orcid.org/0000-0001-6338-2606

References

[1] Poolperm P, Nakkiew W and Naksuk N 2021 Experimental investigation of additive manufacturing using a hot-wire plasma welding process on titanium parts *Materials.* **14** 1270
[2] Ramalho A, Santos T G, Bevans B, Smoqi Z, Rao P and Oliveira J P 2022 Effect of contaminations on the acoustic emissions during wire and arc additive manufacturing of 316L stainless steel *Additive Manufacturing.* **51** 102585
[3] Song Y A, Park S, Choi D and Jee H 2005 3D welding and milling: I. A direct approach for freeform fabrication of metallic prototypes *Int. J. Mach. Tools Manuf.* **45** 1057–62
[4] Ke W C, Oliveira J P, Cong B Q, Ao S S, Qi Z W, Peng B and Zeng Z 2022 Multi-layer deposition mechanism in ultra high-frequency pulsed wire arc additive manufacturing (WAAM) of NiTi shape memory alloys *Additive Manuf.* **50** 102513
[5] Parvizi S, Hashemi S M, Asgarinia F, Nematollahi M and Elahinia M 2021 Effective parameters on the final properties of NiTi-based alloys manufactured by powder metallurgy methods: A review *Prog. Mater Sci.* **117** 100739

[6] Wu B, Ding D, Pan Z, Cuiuri D, Li H, Han J and Fei Z 2017 Effects of heat accumulation on the arc characteristics and metal transfer behavior in Wire Arc Additive Manufacturing of Ti6Al4V *J. Mater. Process. Technol.* **250** 304–12
[7] Moreira A F, Ribeiro K S, Mariani F E and Coelho R T 2020 An initial investigation of tungsten inert gas (TIG) torch as heat source for additive manufacturing (AM) process *Procedia Manuf.* **48** 671–77
[8] Ma Y, Cuiuri D, Hoye N, Li H and Pan Z 2015 The effect of location on the microstructure and mechanical properties of titanium aluminides produced by additive layer manufacturing using *in situ* alloying and gas tungsten arc welding *Mater. Sci. Eng. A* **631** 230–40
[9] Martina F, Mehnen J, Williams S W, Colegrove P and Wang F 2012 Investigation of the benefits of plasma deposition for the additive layer manufacture of Ti–6Al–4V *J. Mater. Process. Technol.* **212** 1377–86
[10] González J, Rodríguez I, Prado-Cerqueira J L, Diéguez J L and Pereira A 2017 Additive manufacturing with GMAW welding and CMT technology *Procedia Manuf.* **13** 840–7
[11] Ding D, Shen C, Pan Z, Cuiuri D, Li H, Larkin N and van Duin S 2016 Towards an automated robotic arc-welding-based additive manufacturing system from CAD to finished part *Computer-Aided Design.* **73** 66–75
[12] Galarraga H, Warren R J, Lados D A, Dehoff R R, Kirka M M and Nandwana P 2017 Effects of heat treatments on microstructure and properties of Ti-6Al-4V ELI alloy fabricated by electron beam melting (EBM) *Mater. Sci. Eng. A* **685** 417–28
[13] Liu W, Liu S, Ma J and Kovacevic R 2014 Real-time monitoring of the laser hot-wire welding process *Opt. Laser Technol.* **57** 66–76
[14] Murr L E, Gaytan S M, Ceylan A, Martinez E, Martinez J L, Hernandez D H and Wicker R B 2010 Characterization of titanium aluminide alloy components fabricated by additive manufacturing using electron beam melting *Acta Mater.* **58** 1887–94
[15] Chadha U, Abrol A, Vora N P, Tiwari A, Shanker S K and Selvaraj S K 2022 Performance evaluation of 3D printing technologies: a review, recent advances, current challenges, and future directions *Progress in Additive Manuf.* **7** 1–34
[16] Conde F F, Avila J A, Oliveira J P, Schell N, Oliveira M F and Escobar J D 2021 Effect of the as-built microstructure on the martensite to austenite transformation in a 18Ni maraging steel after laser-based powder bed fusion *Additive Manuf.* **46** 102122
[17] Ding J, Colegrove P, Mehnen J, Ganguly S, Almeida P S, Wang F and Williams S 2011 Thermo-mechanical analysis of wire and arc additive layer manufacturing process on large multi-layer parts *Comput. Mater. Sci.* **50** 3315–22
[18] Mueller D H and Mueller H 2000 Experiences using rapid prototyping techniques to manufacture sheet metal forming tools *Proc. ISATA Conf. Dublin* 9, 25–27 (https://citeseerx.ist.psu.edu/viewdoc/download?doi=10.1.1.122.2370&rep=rep1&type=pdf)
[19] King D and Tansey T 2003 Rapid tooling: selective laser sintering injection tooling *J. Mater. Process. Technol.* **132** 42–8
[20] Ding D, Pan Z, Cuiuri D and Li H 2015 Wire-feed additive manufacturing of metal components: technologies, developments and future interests *Int. J. Adv. Manuf. Technol.* **81** 465–81
[21] Barsoum Z 2008 Residual stress analysis and fatigue of multi-pass welded tubular structures *Eng. Fail. Anal.* **15** 863–74
[22] Stavinoha J N 2012 Investigation of plasma arc welding as a method for the additive manufacturing of titanium-(6) aluminum-(4) vanadium alloy components. *Montana Tech of The University of Montana* The University of Montana (https://www.proquest.com/openview/4d9949eed4e1ae508da82ce2ffaa9709/1?pq-origsite=gscholar&cbl=18750)
[23] Wang J F, Sun Q J, Wang H, Liu J P and Feng J C 2016 Effect of location on microstructure and mechanical properties of additive layer manufactured Inconel 625 using gas tungsten arc welding *Mater. Sci. Eng. A* **676** 395–405
[24] Hori K, Watanabe H, Myoga T and Kusano K 2004 Development of hot wire TIG welding methods using pulsed current to heat filler wire–research on pulse heated hot wire TIG welding processes *Weld. Int.* **18** 456–68
[25] Lv S X, Tian X B, Wang H T and Yang S Q 2007 Arc heating hot wire assisted arc welding technique for low resistance welding wire *Sci. Technol. Weld. Joining* **12** 431–5
[26] Sun Z and Kuo M 1999 Bridging the joint gap with wire feed laser welding *J. Mater. Process. Technol.* **87** 213–22
[27] Kota K, Kenji S, Motomichi Y and Daisuke T 2011 Development of a high-efficiency/high-quality hot-wire laser fillet welding process *Trans. JWRI.* **39** 47–9
[28] Specialty Metals Titanium Properties Sheet. Available online: (http://specialtymetals.com.au/uploads/5/3/6/6/53662743/specialty-metals-titanium-properties-2018-v1.pdf) (accessed on 2020)
[29] Titanium Grade 2, Chemical Properties Sheet. Available online: (https://titanium.co.th/material/grade_2.html) (accessed on 2021)
[30] American Society for Testing Materials 2013 *Standard Specification for Titanium and Titanium Alloy Wire; ASTM* (West Conshohocken, PA: ASTM International) B863–2014
[31] Nouari M and Makich H 2014 On the physics of machining titanium alloys: interactions between cutting parameters, microstructure and tool wear *Metals.* **4** 335–58
[32] Kadoi K, Shinozaki K, Yamamoto M, Takayanagi D, Nishimoto A, Owaki K and Inose K 2010 Development of a high-efficiency/high-quality hot-wire laser fillet welding process *Transactions of JWRI.* **39** 47–9 chrome-extension://efaidnbmnnnibpcajpcglclefindmkaj/https://ir.library.osaka-u.ac.jp/repo/ouka/all/4436/jwri39_02_047.pdf
[33] Zhu S, Nakahara Y, Aono H, Ejima R and Yamamoto M 2021 Derivation of appropriate conditions for additive manufacturing technology using hot-wire laser method *Materials Proc. Multidisciplinary Digital Publishing Institute* 3, 9
[34] Visual inspection: VT, Website: (https://slideshare.net/champakul/1-1-33037395) (accessed on 2021)
[35] Alcisto J, Enriquez A, Garcia H, Hinkson S, Hahn M, Foyos J and Es-Said O S 2004 The effect of thermal history on the color of oxide layers in titanium 6242 alloy *Eng. Fail. Anal.* **11** 811–16
[36] Peng W, Zeng W, Zhang Y, Shi C, Quan B and Wu J 2013 The effect of colored titanium oxides on the color change on the surface of Ti-5Al-5Mo-5V-1Cr-1Fe alloy *J. Mater. Eng. Perform.* **22** 2588–93
[37] Mok S H, Bi G, Folkes J and Pashby I 2008 Deposition of Ti–6Al–4V using a high power diode laser and wire *Part I: Investigation on the process characteristics. Surface and Coatings Technology.* **202** 3933–9
[38] Mortello M and Casalino G 2021 Transfer mode effects on Ti6Al4V wall building in wire laser additive manufacturing *Manufacturing Letters.* **28** 17–20
[39] Welding, Website: (https://engfanatic.tumcivil.com/tumcivil_1/media/Welding/Welding.pdf), (accessed on 2021)
[40] Sames W J, List F A, Pannala S, Dehoff R R and Babu S S 2016 The metallurgy and processing science of metal additive manufacturing *Int. Mater. Rev.* **61** 315–60
[41] Lin J, Lv Y, Liu Y, Sun Z, Wang K, Li Z and Xu B 2017 Microstructural evolution and mechanical property of Ti-6Al-4V wall deposited by continuous plasma arc additive manufacturing without post heat treatment *J. Mech. Behav. Biomed. Mater.* **69** 19–29
[42] Portable x-ray Residual Stress Analyzer, Available online: (https://pulstec.co.jp/en/product/x-ray/) (accessed on 2021)
[43] Tanaka K 2019 The cosα method for x-ray residual stress measurement using two-dimensional detector *Mechanical Engineering Reviews.* **6** 18–00378
[44] Delbergue D, Texier D, Lévesque M and Bocher P 2016 Comparison of two x-ray residual stress measurement methods: Sin2 ψ and cos α, through the determination of a martensitic steel x-ray elastic constant *In Residual Stresses 2016: ICRS-10.* **2** 55–60

[45] Slotwinski J A and Garboczi E J 2014 Porosity of additive manufacturing parts for process monitoring *AIP conference proceedings* 581 (American Institute of Physics) 1197–204
[46] Slotwinski J A, Garboczi E J and Hebenstreit K M 2014 Porosity measurements and analysis for metal additive manufacturing process control *J. Res. Nat. Inst. Stand. Technol.* **119** 494
[47] Gu J, Cong B, Ding J, Williams S W and Zhai Y 2014 Wire + arc additive manufacturing of aluminium *Proc. of the 25th Annual Int. Solid Freeform Fabrication Symp. Austin TX USA* 4–6
[48] An Introduction to Wire Arc Additive Manufacturing, Available online: (https://amfg.ai/2018/05/17/an-introduction-to-wire-arc-additive-manufacturing/) (accessed on 2021)
[49] Gu J, Ding J, Williams S W, Gu H, Bai J, Zhai Y and Ma P 2016 The strengthening effect of inter-layer cold working and post-deposition heat treatment on the additively manufactured Al–6.3 Cu alloy *Mater. Sci. Eng. A* **651** 18–26
[50] Aiyiti W, Zhao W, Lu B and Tang Y 2006 Investigation of the overlapping parameters of MPAW-based rapid prototyping *Rapid Prototyping Journal* **12** 165–72
[51] Titanium alloy grade 2, Available online: (https://titanium.co.th/material/grade_2.html) (accessed on 2021)
[52] Specialty Metals Titanium-Stainless-Exotic, Available online: (http://specialtymetals.com.au/uploads/5/3/6/6/53662743/specialty-metals-titanium-properties-2018-v1.pdf) (accessed on 2020)
[53] Uhlmann E, Kersting R, Klein T B, Cruz M F and Borille A V 2015 Additive manufacturing of titanium alloy for aircraft components *Procedia Cirp.* **35** 55–60
[54] Wang X and Chou K 2018 Effect of support structures on Ti-6Al-4V overhang parts fabricated by powder bed fusion electron beam additive manufacturing *J. Mater. Process. Technol.* **257** 65–78
[55] Sun R, Li L, Zhu Y, Guo W, Peng P, Cong B and Liu L 2018 Microstructure, residual stress and tensile properties control of wire-arc additive manufactured 2319 aluminum alloy with laser shock peening *J. Alloys Compd.* **747** 255–65
[56] Attar H, Bermingham M J, Ehtemam-Haghighi S, Dehghan-Manshadi A, Kent D and Dargusch M S 2019 Evaluation of the mechanical and wear properties of titanium produced by three different additive manufacturing methods for biomedical application *Mater. Sci. Eng. A* **760** 339–45
[57] Herrmann K 2011 Hardness *Testing: principles and applications* (ASM international)
[58] Baufeld B and Van der Biest O 2009 Mechanical properties of Ti-6Al-4V specimens produced by shaped metal deposition *Sci. Technol. Adv. Mater.* **10** 1–10
[59] Wang F, Williams S, Colegrove P and Antonysamy A A 2013 Microstructure and mechanical properties of wire and arc additive manufactured Ti-6Al-4V *Metallurgical and materials transactions A.* **44** 968–77
[60] Liu S and Shin Y C 2019 Additive manufacturing of Ti6Al4V alloy: A review *Mater. Des.* **164** 107552
[61] Luo K Y, Liu B, Wu L J, Yan Z and Lu J Z 2016 Tensile properties, residual stress distribution and grain arrangement as a function of sheet thickness of Mg–Al–Mn alloy subjected to two-sided and simultaneous LSP impacts *Appl. Surf. Sci.* **369** 366–76
[62] Martina F, Williams S W and Colegrove P A 2013 Improved microstructure and increased mechanical properties of additive manufacture produced Ti-6Al-4V by interpass cold rolling *24th Int. Solid Freeform Fabrication Symp. 12–14 August 2013* 490–96
[63] Schajer G S 1988 Measurement of non-uniform residual stresses using the hole-drilling method *Journal of Engineering Materials and Technology* **110** 338–43
[64] Hoye N, Li H J, Cuiuri D and Paradowska A M 2014 Measurement of residual stresses in titanium aerospace components formed via additive manufacturing *In Materials Science Forum. Trans Tech Publications Ltd* **777** 124–9
[65] DebRoy T, Wei H L, Zuback J S, Mukherjee T, Elmer J W, Milewski J O and Zhang W 2018 Additive manufacturing of metallic components–process, structure and properties *Prog. Mater Sci.* **92** 112–224
[66] Martukanitz R, Michaleris P, Palmer T, DebRoy T, Liu Z K, Otis R and Chen L Q 2014 Toward an integrated computational system for describing the additive manufacturing process for metallic materials *Additive Manuf.* **1** 52–63
[67] Coules H E, Colegrove P, Cozzolino L D, Wen S W and Kelleher J F 2013 High pressure rolling of low carbon steel weld seams: Part 2–roller geometry and residual stress *Sci. Technol. Weld. Joining* **18** 84–90